Remote Sens. **2014**, *6*, 10913-10930; doi:10.3390/rs61110913

OPEN ACCESS

remote sensing

ISSN 2072-4292

www.mdpi.com/journal/remotesensing

Article

Emissivity Measurements of Foam-Covered Water Surface at L-Band for Low Water Temperatures

En-Bo Wei [1,*], Shu-Bo Liu [1,2,†], Zhen-Zhan Wang [3,†], Xiao-Lin Tong [2,3,†], Shuai Dong [2,3,†], Bin Li [3,†] and Jing-Yi Liu [3,†]

[1] Institute of Oceanology, Chinese Academy of Sciences, Qingdao 266071, China; E-Mail: liushubo163@163.com

[2] University of Chinese Academy of Sciences, Beijing 100039, China; E-Mails: tongxl@henu.edu.cn (X.-L.T.); dongshuaihy@sina.com (S.D.)

[3] Centre for Space Science and Applied Research, Chinese Academy of Sciences, Beijing 100190, China; E-Mails: wangzhenzhan@mirslab.cn (Z.-Z.W.); libin@mirslab.cn (B.L.); liujingyi@mirslab.cn (J.-Y.L.)

† These authors contributed equally to this work.

* Author to whom correspondence should be addressed; E-Mail: ebwei@qdio.ac.cn; Tel.: +86-532-8289-8852; Fax: +86-532-8289-8506.

External Editors: Raphael M. Kudela and Prasad S. Thenkabail

Received: 30 June 2014; in revised form: 22 September 2014 / Accepted: 4 November 2014 / Published: 7 November 2014

Abstract: For a foam-covered sea surface, it is difficult to retrieve sea surface salinity (SSS) with L-band brightness temperature (1.4 GHz) because of the effect of a foam layer with wind speeds stronger than 7 m/s, especially at low sea surface temperature (SST). With foam-controlled experiments, emissivities of a foam-covered water surface at low SST (−1.4 °C to 1.7 °C) are measured for varying SSS, foam thickness, incidence angle, and polarization. Furthermore, a theoretical model of emissivity is introduced by combining wave approach theory with the effective medium approximation method. Good agreement is obtained upon comparing theoretical emissivities with those of experiments. The results indicate that foam parameters have a strong influence on increasing emissivity of a foam-covered water surface. Increments of experimental emissivities caused by foam thickness of 1 cm increase from about 0.014 to 0.131 for horizontal polarization and 0.022 to 0.150 for vertical polarization with SSS increase and SST decrease. Contributions of the interface between the foam layer and water surface to

the foam layer emissivity increments are discussed for frequencies between 1 and 37 GHz.

Keywords: sea foam layer; microwave emissivity; L-band; sea surface salinity and temperature

1. Introduction

Passive microwave measurements of sea surface brightness temperatures allow retrievals of geophysical variables, such as wind speed, sea surface salinity (SSS), and sea surface temperature (SST). The Aquarius Mission and European Soil Moisture and Ocean Salinity Mission [1,2] are prime examples. However, under high wind speeds, the foam layer produced by wave breaking over a sea surface always affects the microwave emissive brightness temperature, because foam permittivity is different from that of seawater [3,4]. To adequately account for foam effects on brightness temperature or emissivity, one needs to understand the microwave electromagnetic properties of a foam layer, such as permittivity and emissivity. In fact, these two complex properties are not only related to foam microstructure parameters such as air volume fraction (AVF), foam layer thickness and size of seawater-coated air bubbles, but also microwave frequency, SST and SSS [5–11]. Although the sea foam layer can increase sea surface emissivity [12], this mechanism is not clearly understood, especially in calculating or predicting emissivity and permittivity of that layer.

Recently, much research has focused on foam permittivity and emissivity through both experimental and theoretical investigation, toward developing a specific forward geophysical model of ocean remote sensing. Over the sea surface, the sea foam layer is an aggregation of seawater-coated air bubbles and free water between interstitial spaces of air bubbles [13–15]. Therefore, several effective media approximations (EMA) have been developed to quantitatively calculate the effective permittivity of a foam layer for microwave wavelengths greater than mean air bubble size [16–19]. For example, considering the interactions of dense coated spherical particles, Liu *et al.* [20] developed Rayleigh method to predict the effective permittivity of a foam layer at different microwave frequencies. Anguelova [3] systematically investigated well-known effective permittivity formulae of composite media according their applicability to the sea foam layer. To investigate the emissivity increment induced by a foam-covered sea surface, theoretical models [8–11,16–21] were developed with electromagnetic wave theory, microwave vector radiative transfer equation (VRTE), and EMA theory. For instance, Guo *et al.* [17] investigated the influence of foam microstructures, microwave frequency and foam-layer thickness on the emissivity of a foam-covered sea surface with quasi-crystalline approximation and VRTE, by treating the foam as densely packed air bubbles coated with seawater. To disclose the effects of other foam parameters, such as the ratio of coated air bubbles' inner to outer radii, coherent wave interaction, and sticky force parameter on foam emissivities, microwave radiative transfer theory has also been applied to the foam layer [7,9,22,23]. For the AVF with vertical distribution in a foam layer, Wei [10] proposed an EMA method to estimate foam emissivity of a non-uniform AVF. Similarly, Anguelova *et al.* [5] and Raizer [21] presented a radiative transfer model for estimating the emissivity of a vertically structured foam layer at microwave frequencies. Although the

aforementioned theoretical models have demonstrated the influence of foam structures on emissivity, it is still difficult to calculate foam layer emissivity.

To improve the accuracy of theoretical models and obtain more experimental data on foam layers, various controlled experiments of foam-covered sea surfaces have been recently conducted to measure the emissivity and geometric parameters of those layers, such as bubble size distribution, coating thickness, foam thickness, and AVF [6]. As an example, at 10.8 GHz and 36.5 GHz, Rose *et al.* [8] obtained a formula of foam emissivity by means of a power-series polynomial of incidence angles for foam thickness 2.8 cm. To investigate effects of breaking waves and the foam layer on sea surface brightness temperatures, Padmanabhan *et al.* [24] conducted an emissivity experiment of the wave-breaking surface at 10.8, 18.7, and 37 GHz. With experiments on various foam shapes and foam-water interfaces, Williams [25] showed that the meniscus of the foam–water interface can contribute a significant fraction of foam emissivity increments at 9.2 GHz. With an artificial foam experiment at 37.5 GHz, Millitskii [26] revealed that the major contributor to foam emissivity increase is the thin monolayer of bubbles near the foam-water interface. To address the effects of SST and foam thickness on foam emissivity at 6.8 GHz, Wei *et al.* [11] conducted an experiment with a completely foam-covered surface, obtaining averaged emissivity increments, with foam thickness of 1 cm, from 0.25 to 0.35 for both horizontal (H) and vertical (V) polarizations at incidence angles from 20° to 40°. To eliminate foam layer influences on SSS retrieval at L-band (1.4 GHz), Camps *et al.* [6] carried out a specific experiment to measure foam emissivity for various SSSs and higher SSTs (≥ 14 °C). The above experiments were conducted at water temperatures of 10 °C–30 °C. There have been few experiments focused on emissivity at low SST.

For remote sensing of SSS, because the absolute value of the sensitivity of brightness temperature at 1.4 GHz to SSS declines with decreasing SST, SST is a key parameter affecting SSS retrieval [27–29]. Moreover, in high-latitude ocean regions, SST is low, from −2 °C to 5 °C. To develop a theoretical model of a foam-covered sea surface at L-band (1.4 GHz), we performed emissivity experiments of such a surface at low SST for varying SSSs, so that the emissivity increment induced by the foam layer is estimated by various foam factors. Furthermore, based on experimental data on foam parameters, a refractive formula of foam permittivity is determined to simulate measured emissivities using a two-layer emission model derived by the wave approach theory.

2. Measurement Approach

To derive the emissivity of a foam-covered sea surface from measured brightness temperatures of the foam layer and atmospheric downwelling radiation, brightness temperature noise of the foam experimental system was reduced. If brightness temperatures of both foam-free flat and foam-covered water surfaces are measured within a short time, brightness temperature noise T_p^N of the experimental system was estimated with that of the foam-free calm water surface:

$$T_p^N = T_{Bp}^m - \Gamma_p T_p^{sky} - T_{Bp}^c \quad (1)$$

where subscript p = H or V corresponds to H or V polarizations, respectively. T_{Bp}^m is the brightness temperature reached at antenna surface in the flat water experiment. $\Gamma_p = 1 - e_p$ represents the reflectivity of that surface, where e_p is its emissivity, calculated by the Fresnel reflection coefficient.

$T_{Bp}^{c} = e_p SST$ is the theoretical brightness temperature of the calm water surface. T_p^{sky} is the sum of brightness temperatures of the sky and atmospheric downwelling radiation. To derive brightness temperature T_{Bp}^{m} from measured antenna temperature T_A in our experiment, a linear relationship between brightness temperature and measured antenna temperature was defined as $T_{Bp}^{m} = aT_A + b$, where the coefficients a and b were determined by simulated brightness temperature (*i.e.*, T_{Bp}^{m} was calculated by the flat water surface model) and antenna temperature T_A of flat water surface by applying measured antenna pattern. With this relationship, the effect of sidelobes picking radiation from the surroundings was removed. The main beam efficiency of radiometer antenna is 98.36% at whole space integration of antenna radiation pattern, which results that the maximum bias between the brightness temperature of theoretical model and the linear fitting brightness temperature with measured antenna temperature is about 0.1 K. For the case of foam-covered water surface, the above linear relationship between brightness temperature and measured antenna temperature was applied to derive the brightness temperature of foam-covered surface.

In the foam generation procedure, the foam generating area (Figure 1b) is the sum of foam region "A" (*i.e.*, water-coated air bubbles over the water surface) and air-water mixture region "B" (*i.e.*, air bubbles immersed in water). Foam coverage fraction w_1 and air-water mixture coverage fraction w_2 were calculated with the foam generating area and L-band automatic radiometer (LBAR) antenna-boresighted area over the experimental water surface at different incidence angles. Then, the coverage fraction of the foam-free water surface was $1 - w_1 - w_2$. Brightness temperature T_p^F reached at antenna surface includes the brightness temperatures of the foam-generating region, seawater region, and the reflected sky and atmospheric downwelling radiation:

$$T_p^F = w_1 e_p^F SST + w_2 e_p^{mixt} SST + (1 - w_1 - w_2) T_{Bp}^{c} + \Gamma_p^F T_p^{sky} + T_p^N \quad (2)$$

where the first two terms on the right side of the equation are brightness temperatures of the foam-covered and air-water mixture surfaces, respectively. e_p^F and e_p^{mixt} are emissivities of the foam and air-water mixture regions, respectively. The third term is the brightness temperature contribution of the foam-free water surface. The fourth term results from the total brightness temperature of the reflected sky and atmosphere downwelling radiation by the experimental water surface, where reflectivity Γ_p^F of the foam experiment surface is calculated by $\Gamma_p^F = 1 - w_1 e_p^F - w_2 e_p^{mixt} - (1 - w_1 - w_2) e_p$. Substituting the noise brightness temperature T_p^N of Equation (1) into Equation (2), emissivity of the foam-covered surface was estimated by

$$e_p^F = \frac{T_p^F - T_{Bp}^m}{w_1 (SST - T_p^{sky})} + e_p + \frac{w_2}{w_1}(e_p - e_p^{mixt}) \quad (3)$$

where the unknown emissivity e_p^{mixt} of the air-water mixture can be calculated by the following method. Because the microwave wavelength of L-band (1.4 GHz) is larger than the size of air bubbles in the air-water mixture, that mixture is regarded as an effective medium. Then, the effective permittivity ε_e of the mixture is estimated by the Maxwell-Garnett Equation (4) of the spherical composite (*i.e.*, air bubbles embedded in seawater) [30]:

$$\varepsilon_e = \varepsilon_w (1 + 2 b_0 f_{aw}) / (1 - b_0 f_{aw}) \quad (4)$$

where $b_0 = (\varepsilon_a - \varepsilon_w)/(\varepsilon_a + 2\varepsilon_w)$ and ε_a and ε_w are the dielectric constants of air and seawater, respectively. The seawater dielectric constant is a function of microwave frequency, SST and SSS [31]. The AVF f_{aw} of the air-water mixture was extracted by Equation (4), for which effective conductivities of the air-water mixture and seawater were measured with a conductivity instrument. Note that the conductivity and permittivity are interchangeable in that equation. Furthermore, it is assumed that the air-water mixture surface is flat. Emissivity e_p^{mixt} is estimated by the Fresnel reflection coefficient.

Figure 1. Photography of foam emissivity experiment: (**a**) experimental scene; (**b**) image of foam region (denoted by "A") and air-water mixture region (region denoted by "B"); (**c**) top view of air bubble size; (**d**) side view of foam thickness and air bubble size.

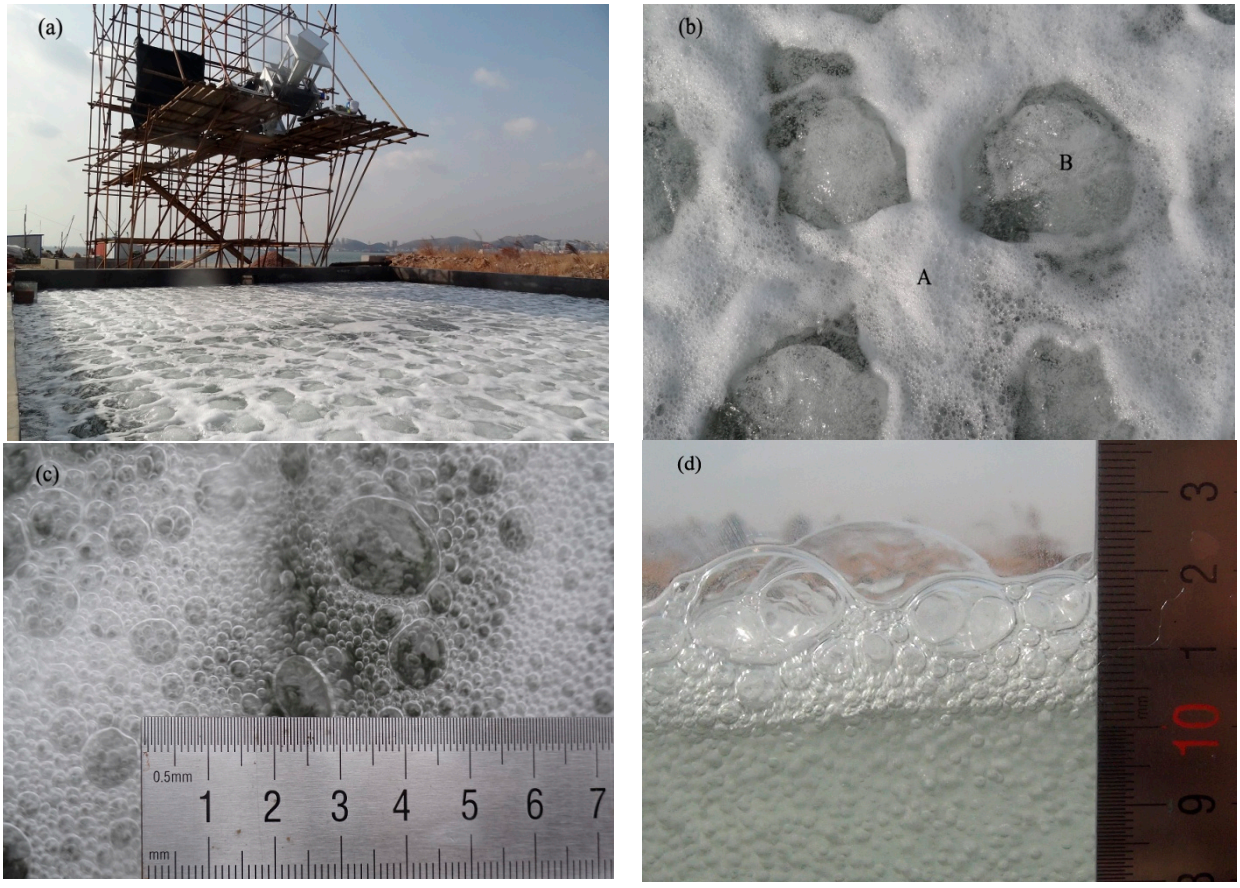

In Equation (3), the following parameters were measured and inferred from measured data: (1) brightness temperature T_p^F reached at antenna surface derived in the foam experiment, *i.e.*, the sum of brightness temperatures of the foam generating region, seawater region, and the reflected sky and atmosphere downwelling radiation; (2) total brightness temperature T_p^{sky} of the sky and atmosphere downwelling radiation; (3) brightness temperature T_{Bp}^m reached at antenna surface in the flat water surface experiment; (4) foam thickness, air bubble size, SSS and SST measured by video camera and A7CT sensors; (5) conductivities of the air-water mixture and seawater, used to estimate AVF f_{aw} of the air-water mixture; (6) emissivity e_p^{mixt}, calculated by the Fresnel reflection coefficient and Equation (4); (7) the sum of w_1 and w_2, calculated by the antenna height above the water surface,

incidence angle, and antenna solid angle; (8) the ratio of w_1 to w_2, estimated by analyzing photos of the foamy surfaces; (9) AVF of the foam layer, output by the theoretical emissivity models.

3. Experiment Description

A foam emission experiment was conducted in December 2012 at Tangdao Bay of Qingdao, to measure foam emissivity with the LBAR designed by the National Space Science Center of the Chinese Academy of Sciences. The LBAR was installed on a trestle platform of height 4.5 m over a foam-covered water pool of length 32 m, width 11 m, and depth 1.2 m. The LBAR height ensured far-field conditions for the conic antenna size of bore diameter 0.5 m (Figure 1a). Incidence angle was automatically recorded by the radiometer control system. The LBAR had a dual-polarization (V and H) 25° antenna half-power beam width with sensitivity 0.2 K (Kelvin) and integration time 1 s. With a hot load in a temperature-controlled box coupled with a noise source and cold reference at ambient temperature, combined with an outside microwave absorber and cold space, on-site calibration error of brightness temperature was less than 1 K for a flat sea surface.

Foam generators fixed under the bottom of the water pool were of length 12 m and width 11 m. During the experiment, a Sony DSC-HX7 digital camera and Sony HDR-PJ50E video camera were used to record the foam generation area, foam thickness, and bubble sizes in the foam layer (Figure 1b–d). SST was −1.4 °C to 1.7 °C, and SSS was controlled by sea salt, with salinity between 31 and 38 psu. Conductivity and temperature sensors of an Infinity-A7CT (JFE Advantech Co. Ltd., Kobe, Japan) were used to measure SST, SSS, and conductivities of seawater and air-water mixtures. Mean diameter of measured air bubbles within the foam layer was about 1.6 mm. The foam generation area (Figure 1b) was calculated by the incidence angle, microwave beamwidth, and antenna height. The ratio of w_1 to w_2 was statistically estimated at ~1.2 by analyzing areas of the foam and air-water mixture regions in photos of the foam generation surfaces. Effective conductivities of the air-water mixture and seawater were measured with the conductivity instrument and were used to retrieve the AVF f_{aw} (*i.e.*, retrieved value $f_{aw} = 0.05$ in our experiments) of the former mixture using Equation (4). For each experiment with variable SST and SSS, the two measurements of the flat water and foam-covered surfaces were completed within an hour. First, brightness temperatures of the calm water surface, sky and atmosphere downwelling radiation were measured within the first half hour at different incidence angles, when the antenna scanned the water surface and sky (*i.e.*, including the atmospheric downwelling radiation and attenuated cosmic radiation brightness temperature), respectively. Similarly, brightness temperatures of the foam-covered water surface and sky downwelling radiation were measured within the last half hour. Here, the average brightness temperature T_p^{sky} for each experiment was used in Equation (3).

4. Theoretical Emissivity Model

To seek a theoretical emissivity model of the foam-covered water surface, we regarded the foam as a medium consisting of densely packed air bubbles embedded in the seawater. The foam-covered surface can be modeled by three layers. These are the air layer on top (Layer 0), foam layer in the middle (Layer 1), and seawater at the bottom (Layer 2), for which the interfaces between each layer are assumed

flat. With the wave approach theory of a two-layer medium [32], emissivity $e_p^{F,T}$ of the foam-covered sea surface is calculated as

$$e_p^{F,T} = 1 - \left| R_p^{foam} \right|^2 \tag{5}$$

where the reflection coefficient R_p^{foam} of the foam-covered sea surface is calculated by $R_p^{foam}(\theta_i) = \dfrac{R_p^{01}(\theta_i)e^{i2\Psi} + R_p^{12}(\theta_i)}{e^{i2\Psi} + R_p^{01}(\theta_i)R_p^{12}(\theta_i)}$. Here, $\Psi = \dfrac{2\pi d}{\lambda_0}\sqrt{\varepsilon_e - \sin^2\theta_i}$ is an attenuation factor, λ_0 is the microwave wavelength in free space, and d and θ_i are the foam layer thickness and incidence angle, respectively. $R_p^{nm}(\theta_i)$ represents the Fresnel reflection coefficients from layers *n* to *m*:

$$R_h^{01}(\theta_i) = \frac{\cos\theta_i - \sqrt{\varepsilon_e - \sin^2\theta_i}}{\cos\theta_i + \sqrt{\varepsilon_e - \sin^2\theta_i}} \quad R_v^{01}(\theta_i) = \frac{\varepsilon_e\cos\theta_i - \sqrt{\varepsilon_e - \sin^2\theta_i}}{\varepsilon_e\cos\theta_i + \sqrt{\varepsilon_e - \sin^2\theta_i}} \tag{6}$$

$$R_h^{12}(\theta_i) = \frac{\sqrt{\varepsilon_e - \sin^2\theta_i} - \sqrt{\varepsilon_w - \sin^2\theta_i}}{\sqrt{\varepsilon_e - \sin^2\theta_i} + \sqrt{\varepsilon_w - \sin^2\theta_i}} \quad R_v^{12}(\theta_i) = \frac{\varepsilon_w\sqrt{\varepsilon_e - \sin^2\theta_i} - \varepsilon_e\sqrt{\varepsilon_w - \sin^2\theta_i}}{\varepsilon_w\sqrt{\varepsilon_e - \sin^2\theta_i} + \varepsilon_e\sqrt{\varepsilon_w - \sin^2\theta_i}} \tag{7}$$

where the seawater dielectric constant ε_w of low temperature at L-band is given in [31], and ε_e is effective permittivity of the foam layer. Clearly, the emissivities of theoretical Equation (5) are determined by effective permittivity of the foam layer and its thickness. Thus, given that thickness, the foam effective permittivity will be the sole factor in modeling the experimental emissivities. It is well known that there are many effective permittivity formulas of two-phase composites, such as Maxwell-Garnett (MG), refractive model (RM), Looyenga model (LM), and Polder-van Santen model (PSM) [3]. The question is which formula is suitable for modeling our measured emissivities. As a reference, Anguelova [3] theoretically ranked these permittivity formulae according to their applicability to sea foam, in which the three top-ranking formulae were RM (Equation (8)), LM (Equation (9)), and MG (Equation (4)), respectively.

$$\varepsilon_e = [f_a + (1 - f_a)\sqrt{\varepsilon_w}]^2 \tag{8}$$

$$\varepsilon_e = [f_a + (1 - f_a)\varepsilon_w^{1/3}]^3 \tag{9}$$

where f_a is the AVF of the foam layer, which replaces f_{aw} of Equation (4). In these formulae, this AVF is very important for computing emissivities.

To seek the best theoretical model for our experimental emissivities, we constructed a cost function χ^2 by means of the experimental data and theoretical models, so that the valid theoretical model attains the minimum cost function by tuning AVF:

$$\chi^2 = \frac{1}{N}\sum_{i=1}^{N}\{[e_H^F(\theta_i) - e_H^{F,T}(\theta_i)]^2 + [e_V^F(\theta_i) - e_V^{F,T}(\theta_i)]^2\} \tag{10}$$

here, the foam layer AVF in our experiment is unknown. To determine the best theoretical model with the measured data, we should constrain the AVF in Equation (10) because the theoretical emissivity model depends on it. Some references show that the average AVF of an artificial foam layer is larger than 85% [6,8,11], which is different from those of natural sea foam produced by wave breaking, *i.e.*, 55% to 76% [13]. For an example artificial foam experiment, Rose *et al.* [8] found that the AVF is

about 85% in the center of the foam layer, and that on its top surface increases as the foam ages and water drains from bubble interstitial areas. Chen *et al.* [7] showed that the AVF of artificial foam was 80% to 90% in most cases, by analyzing bubble images; an AVF of 90% was adopted for their emissivity model. AVF differences between artificial and natural sea foam layers result from air bubbles continuously aggregating over the sea surface during artificial foam experiments, so that the AVF of the artificial layer is larger than that of the natural layer. Here, the AVF constraint condition greater than 85% was used to select the best theoretical model for our experiment. Based on the theoretical models of Equations (4), (8) and (9), minimum root mean square errors (RMSE) between the experimental and theoretical emissivities are presented in Table 1, along with the tuning AVF f_a of the foam layer. From Table 1, although the minimum RMSEs of the LM emissivity model at both H and V polarizations are smaller than those of the other two models, its average AVF does not meet the AVF constraint condition. Thus, the RM and MG models are valid for our experiments, considering the values of AVF. However, because the RMSEs of the MG model are larger than those of the RM, the latter model was chosen to analyze our experiments. Here, the effect of water and foam surface roughness on the measured brightness temperature is neglected.

Table 1. RMSE between experimental and theoretical emissivities for H and V polarizations, and the tuning AVF f_a of the foam layer.

Model	LM	RM	MG
AVF f_a	0.8377	0.8883	0.9545
RMSE H	0.0079	0.0079	0.0083
RMSE V	0.0103	0.0109	0.0128
RMSE H + V	0.0182	0.0188	0.0211

5. Results and Discussion

5.1. Experimental Results and Theoretical Analyses

The measured foam emissivity was obtained via Equation (3). For the same experimental conditions (SST, SSS, and foam thickness *d*), we modeled foam emissivity using Equation (5) in combination with RM for foam permittivity; hereafter, we refer to this combination of emissivity and permittivity models as the RM emissivity model. We compared measured and modeled foam emissivities and found their strongest agreement by tuning the AVF values (Table 2). Figure 2 shows that the theoretical results are generally in good agreement with measured emissivities at both H and V polarizations for incidence angles from 30° to 59°. By comparing their RMSEs, the H polarization agreement with measured emission data are stronger than those of V polarization. To qualitatively validate the estimated AVF by the RM emissivity model, we analyzed characteristics of AVF variation with SST and SSS, which are shown in Figure 3a,b, respectively. Moreover, from Camps' foam experimental data [6], the AVFs retrieved by the RM emissivity model and Rayleigh method [19] are plotted in Figure 3c,d. Although there are some differences between the AVF values retrieved by the two models from Camps' data, the extracted AVFs have similar trends with SST (or SSS). That is, the AVFs increase (or decrease) with increasing SST (or decreasing SSS). This result implies that AVF increase with SST increase is reasonable in the thermophysics. The emissivities decreasing with SSS increase can be explained by

the mean radius of water-coated air bubbles decreasing non-linearly with increasing SSS in previous foam observations [6,11]. This is because the AVF f_a of a foam layer can be approximated by $f_a \propto (\frac{b-\delta}{b})^3 \approx 1-3\delta/b$, where the constant δ is film thickness of the water coating of an air bubble and b is the outer radius of a coated air bubble.

Table 2. Measured parameters of Figure 2 and tuning AVF used in RM emissivity model.

Experiment	SSS (psu)	SST (°C)	AVF	Foam Thickness (cm)
Figure 2a	31.23	1.66	0.9161	1.18
Figure 2b	31.71	0.20	0.9114	1.35
Figure 2c	32.50	1.56	0.9049	1.42
Figure 2d	32.76	0.92	0.9246	1.35
Figure 2e	33.63	1.52	0.9137	1.50
Figure 2f	34.66	−1.43	0.8768	1.19
Figure 2g	36.50	−1.00	0.8265	1.23
Figure 2h	37.74	0.11	0.8326	1.10

Figure 2. Measured and theoretical emissivities of foam-covered surface *vs.* incidence angle, where "Measured-H" and "Measured-V" are measured horizontal and vertical emissivities, respectively. Theoretical results of RM emissivity model are shown by "Theory-H" and "Theory-V". For each panel, the SSS, SST, foam thickness d, and air volume fraction are listed in Table 2. (**a**) SSS = 31.23 psu, SST = 1.66 °C, d = 1.18 cm, AVF = 0.9161; (**b**) SSS = 31.71 psu, SST = 0.20 °C, d = 1.35 cm, AVF = 0.9114; (**c**) SSS = 32.50 psu, SST = 1.56 °C, d = 1.42 cm, AVF = 0.9049; (**d**) SSS = 32.763 psu, SST = 0.92 °C, d = 1.35 cm, AVF = 0.9246; (**e**) SSS=33.63 psu, SST = 1.52 °C, d = 1.50 cm, AVF = 0.9137; (**f**) SSS = 34.66 psu, SST = −1.43 °C, d = 1.19 cm, AVF = 0.8768; (**g**) SSS = 36.50 psu, SST = −1.00 °C, d = 1.23 cm, AVF = 0.8265; (**h**) SSS = 37.74 psu, SST = 0.11 °C, d = 1.10 cm, AVF = 0.8326.

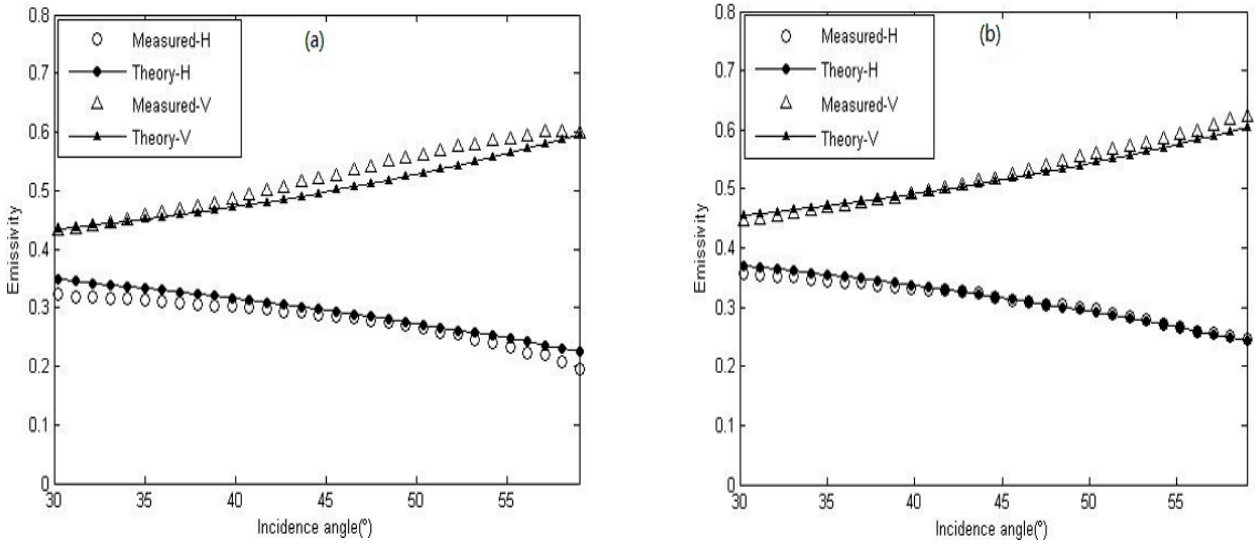

Figure 2. *Cont*.

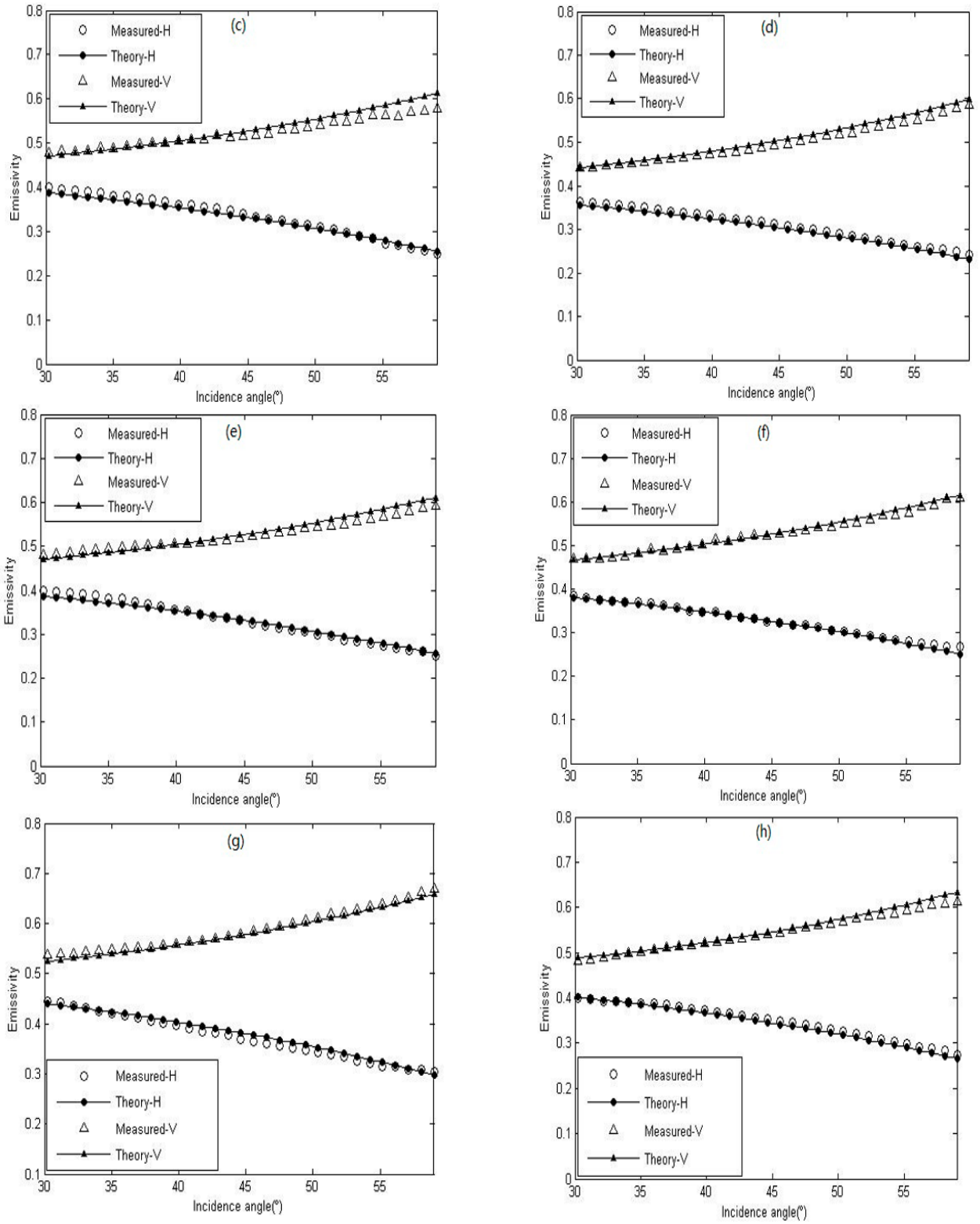

Figure 3. Air volume fraction (AVF) of foam layer *versus* SST and SSS: (**a**) AVF obtained by RM emissivity model in our experiments *versus* SST; (**b**) AVF obtained by RM emissivity model for our experiments *versus* SSS; (**c**) AVF obtained by RM emissivity model and Rayleigh method from Camps' experiments [6] *versus* SST; (**d**) AVF obtained by RM emissivity model and Rayleigh method from Camps' experiments [6] *versus* SSS.

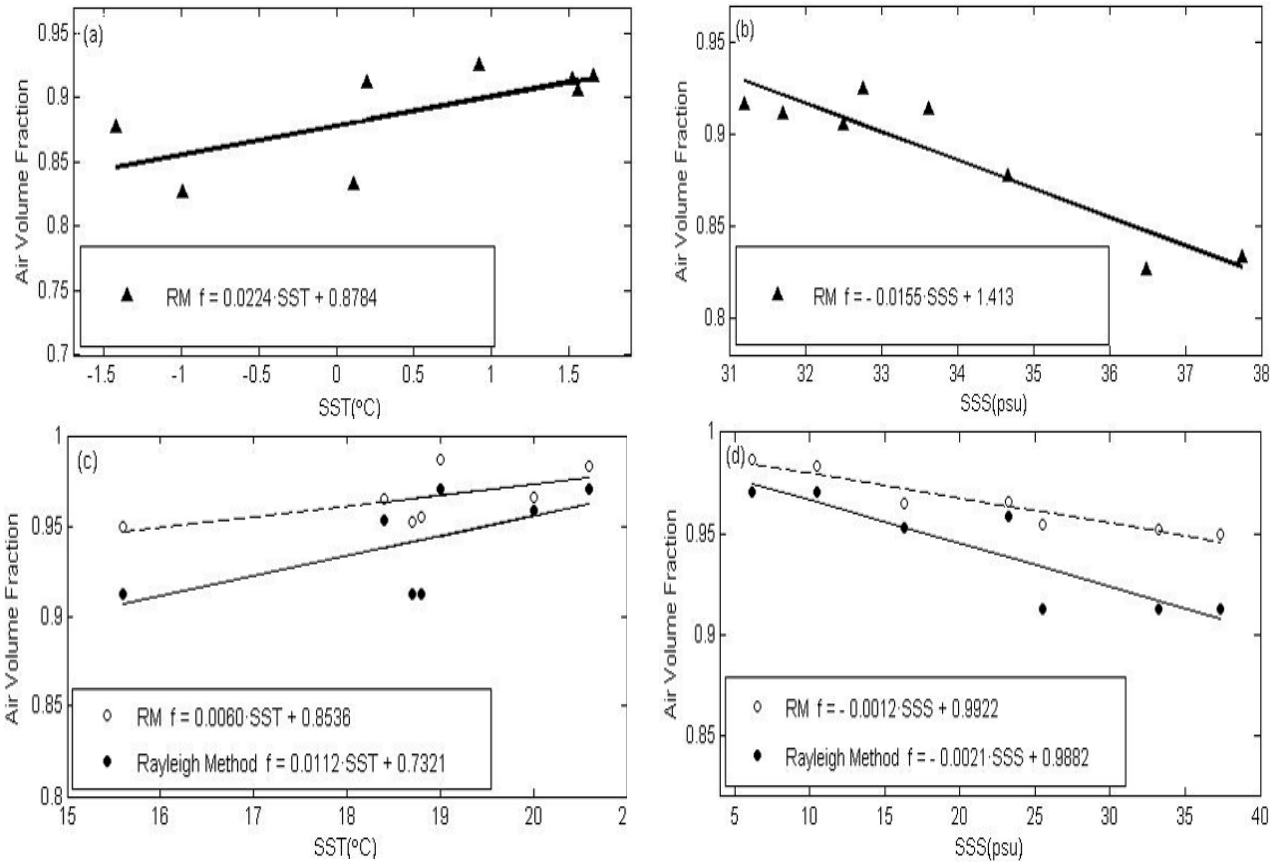

To discern the mechanism of emissivity increment for the foam-covered sea surface, we investigated the effect of a foam factor on foam emissivity using the RM emissivity model, with other factors fixed. For example, with SST 0.5 °C, SSS 34 psu, foam thickness 1.3 cm, AVF 0.9, and incidence angle 35°, sensitivities of the emissivities to SST were about 6.4×10^{-4} (1/°C) and 1.9×10^{-3} (1/°C) for V and H polarizations, respectively. Vertical and horizontal sensitivities of SSS were about 8.0×10^{-4} (1/psu) and 2.6×10^{-3} (1/psu), respectively. Thus, SSS and SST were almost equally important in estimating the foam layer emissivity at low SST. However, the AVF and foam thickness had stronger effects on the emissivities, with vertical (horizontal) sensitivities of emissivities to them around 4.3×10^{-3} (3.5×10^{-2}) (both with units 1/0.01) and 0.021 (0.025) (both with units 1/mm)), respectively. It is clear that the sensitivity of H polarization was larger than that of V polarization. Furthermore, regarding the effect of AVF on foam emissivity with the RM emissivity model, the emissivity decreases (increases) with increasing AVF for AVF greater (less) than 0.7 (Figure 4a). This result indicates that air of the foam layer more strongly controlled foam emissivity than did the water, owing to a large AVF. Figure 4b implies that emissivity of the RM emissivity model generally fluctuated with increasing thickness of the foam layer. Clearly, emissivity rose with initially increase of foam thickness for thickness less than about 3 cm. For thickness greater than 25 cm, saturation emissivity was maintained, for which the threshold of the thickness is related to the microwave wavelength and optical thickness of the foam

composite. The fluctuation characteristic of emissivity for foam thickness 3–25 cm results from the phase coherent effect of the two-layer model [32]. The oscillatory behavior is caused by the coherent addition of the multiple reflections at the air-foam and foam-water boundaries. As foam thickness is increased, the attenuation through the foam medium increases, thereby reducing the magnitude of the reflections from the water surface [33]. However, the emissivity increases with foam thickness up to its saturation value in [7] with an incoherent model [33], which does not exhibit the oscillatory behavior of coherent reflectivity, because it does not account for phase interference effects. Note that emissivity model of wave approach is a coherent model, and its oscillatory magnitude is related to both foam thickness and microwave frequency. In our experiments, the emissivity declined with increasing AVF and decreasing foam thickness, because the AVF was larger than 0.7 and foam thickness was less than 3 cm. From the above theoretical discussion, we conclude that the AVF and foam thickness are key parameters in predicting the emissivity of a foam layer. However, if the foam thickness and AVF vary within a very small range, SSS and SST are important for calculating the emissivity.

Figure 4. Foam emissivity calculated by RM emissivity model at 1.4 GHz *versus* AVF and foam thickness: (**a**) emissivity *versus* AVF for foam thickness d = 1.3 cm, SST = 0.5 °C and SSS = 34 psu; (**b**) emissivity *versus* foam thickness for SST = 0.5 °C, SSS = 34 psu and AVF = 0.9.

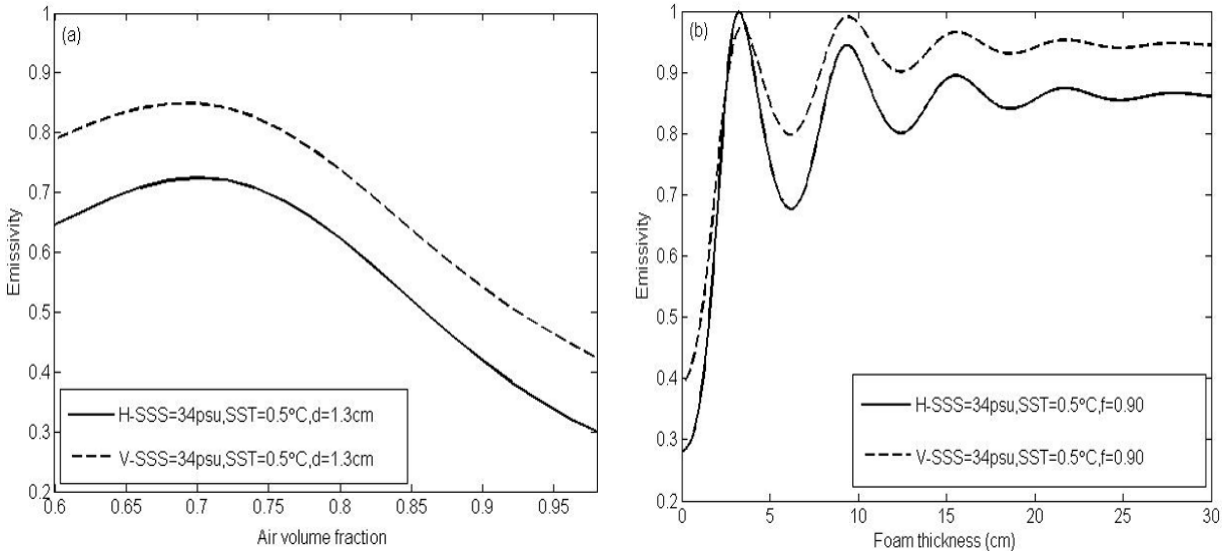

5.2. Emissivity Increments Induced by Foam Layer

Compared with the emissivities of flat sea surfaces, emissivity increments $\Delta e_p = e_p^F - e_p$ of foam-covered water surfaces were calculated with the measured emissivities. In Figure 5, for foam thickness 1 cm and SSS increasing from 31 to 38 psu, average emissivity increments increase from about 0.014 to 0.131 for H polarization and 0.022 to 0.150 for V polarization, respectively. This result is very similar to that of Camps' experiment for higher SST [6]. However, with AVF and SST increase, the emissivity increments of both polarizations generally decrease for the foam thickness fixed at 1 cm. For this thickness in our experiments varying between 1.1 and 1.5 cm, the emissivity increments fluctuated around averages of 0.081 for H polarization and 0.089 for V polarization, under the influences of other

foam factors. Therefore, interactions of foam factors such as AVF, foam thickness, SSS, and SST are also important in estimating the foam emissivity increments. These increments did not clearly depend on incidence angle.

Figure 5. Average emissivity increments $\Delta e_{H,V}$ for foam thickness 1 cm, varying with SSS and incidence angle: (**a**) at horizontal polarization; (**b**) at vertical polarization.

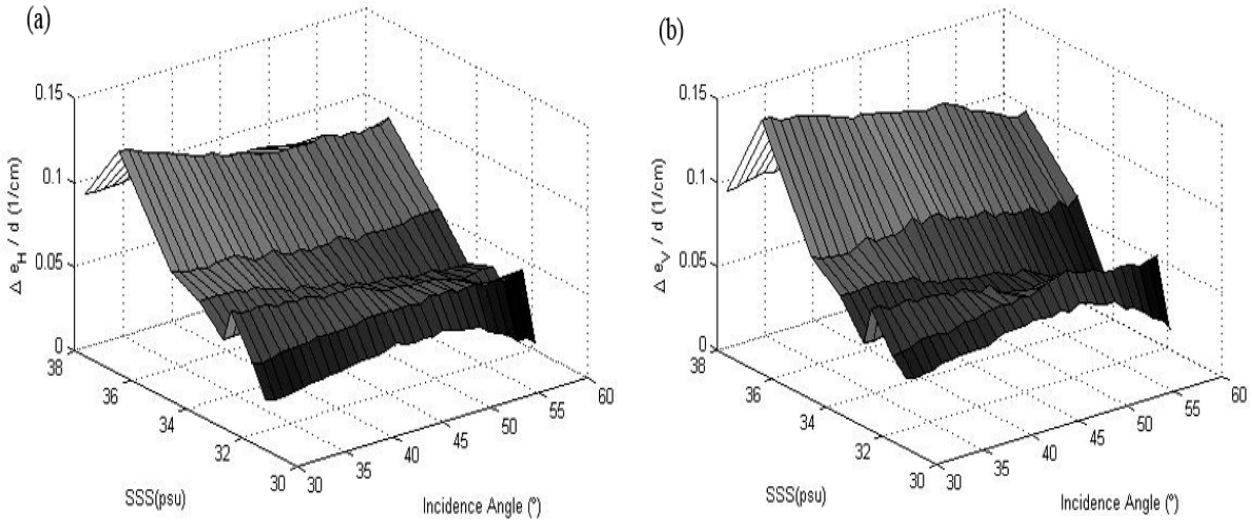

To address effects of the foam layer bottom boundary on the emissivity, some research investigated the influences of a distorted water surface between the foam and water surface [25,34], *i.e.*, the meniscus interface. The contribution of the meniscus zone to the increment of sea foam emissivity depends on the size of air bubbles and microwave frequencies, owing to a gradual transition from permittivity of the air-water mixture (or air) to that of seawater [25]. For example, Anguelova [35] concluded that wet foam near the foam-water interface has a greater impact on emissivity than dry foam at the top of the foam layer. For 6.6 and 10.7 GHz, Wilheit pointed out that a significant fraction of foam emissivity increment comes from the contribution of meniscus interfaces [34]. In the present study, to theoretically investigate the contribution of meniscus to the foam emissivity increment, RM emissivity model was used to estimate emissivity of the meniscus interface from 1 to 37 GHz. For simplicity, the meniscus zone was approximately regarded as a periodic unit cube medium of single-layer dense spherical air bubbles embedded in seawater across the sea surface, where the meniscus zone thickness was around the diameter of an air bubble. The theoretical AVF of the meniscus zone is about $\pi/6$ [11]. Figure 6 shows calculated emissivity increments caused by a meniscus with thickness 1.5 mm (air bubble diameter) and AVF 0.5236, and foam layer thickness 1.3 cm and AVF 0.91; other parameters were SSS = 34 psu, SST = 0.5 °C, and incidence angle = 35°. Clearly, there was a peak emissivity increment $\Delta e_p^{menis} = e_p^{menis} - e_p$ induced by the meniscus at frequency 12 GHz, and the increments increased (or decreased) with frequencies increasing from 1 to 12 GHz (or from 12 to 25 GHz). However, emissivity increments $\Delta e_p^F = e_p^F - e_p$ induced by foam thickness of 1.3 cm had strong fluctuation with microwave frequency, with two maxima of emissivity increments, at 4 and 12 GHz. From the ratios of the emissivity increments Δe_p^{menis} to Δe_p^F varying with frequency, it was found that the meniscus made the largest contributions of 59% and 66% to the foam layer emissivity increments at 8 GHz for H and V polarizations, respectively. For frequencies higher than 20 GHz, the ratios were stable about 36% for H

polarization and 45% for V polarization. However, at 1.4 GHz, the meniscus zone had a small fraction of foam emissivity increments, 7.8% and 8.6% for H and V polarizations, respectively. Generally, from the aforementioned findings, it is concluded that the meniscus transition zone has a stronger effect on foam emissivity increase for microwave frequency higher than 5 GHz. Nevertheless, for complex meniscus structures of a natural sea surface, its emissivity should be further investigated by theoretical and experimental methods.

Figure 6. Emissivity increments induced by foam layer (thickness 1.3 cm and AVF 0.9) and meniscus zone (thickness 1.5 mm and AVF 0.5236) calculated by RM emissivity model. Their ratios vary with microwave frequency, where SST = 0.5 °C, SSS = 34 psu, and incidence angle = 35°.

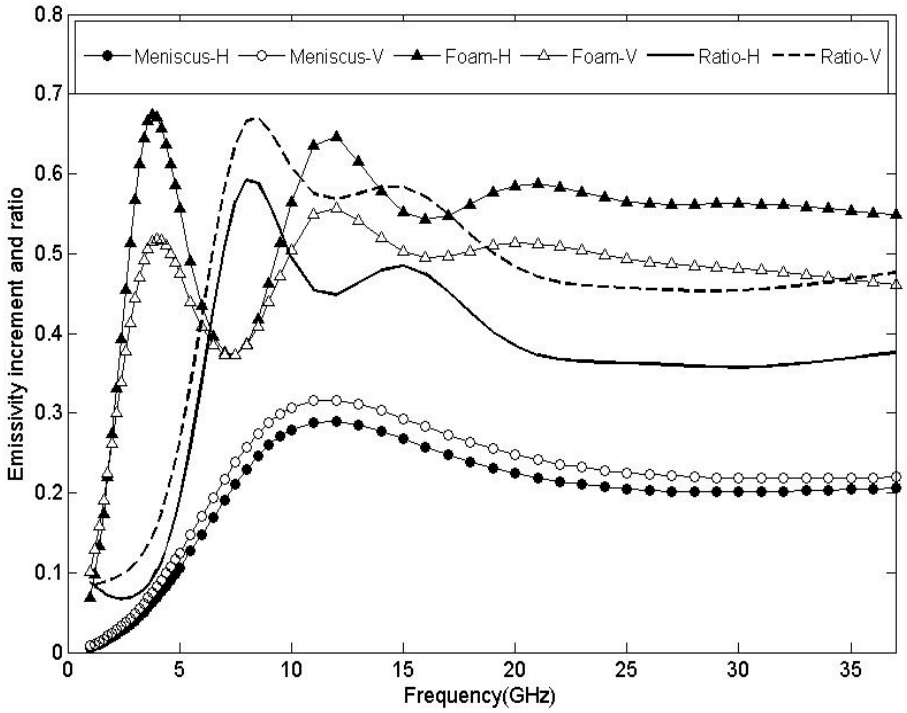

5.3. Effects of Foam Layer on Retrieving Sea Surface Salinity

Considering the natural ocean, the effect of the foam layer on SSS retrieval can be estimated by combining foam coverage fraction w with the emissivity increment of the foam-covered surface, where w depends on wind speed, the air-water temperature difference, and other parameters. As an example, foam coverage fraction on the sea surface is about 1% at (10 m height) wind speed 10.0 m/s [36]. For a flat sea surface with w, the total brightness temperature is

$$\begin{aligned} T_p^{Total} &= (1-w)e_p T_{sea} + we_p^F T_{sea} \\ &= e_p T_{sea} + w\Delta e_p^F T_{sea} \end{aligned} \tag{11}$$

where T_{sea} is sea surface temperature (unit K). For SST = 1.52 °C, SSS = 33.63 psu, foam thickness 1.5 cm, and tuning AVF 0.9137, emissivity increments Δe_p^F in our experiments were about 0.079 for H polarization and 0.083 for V polarization at incidence angle 44.6°. Brightness temperature errors induced by the foam layer were about 0.22 K for the H polarization model and 0.23 K for the V

polarization model for w = 1%, (*i.e.*, the second term on right side of Equation (11)). For the low SST of 1.52 °C and SSS = 33.63 psu, sensitivities of sea surface brightness temperatures to SSS were about 0.21 and 0.31 K/psu for H and V polarizations, respectively. Then, the SSS retrieval errors were about 1.0 and 0.74 psu for H and V polarization models of the flat sea surface, respectively. For comparison to the case of low SST, SSS retrieval errors of higher SST were estimated using the measured emissivity increments (0.098 for H polarization and 0.15 for V polarization) of Figure 11g in [6] for a foam-covered sea surface at incidence angle 45°, where SST = 18.7°C, SSS = 33.21 psu, and foam thickness = 1.665 cm. In this case, sensitivities of sea surface brightness temperatures to SSS were about 0.45 and 0.69 K/psu for H and V polarizations, respectively. For w = 1%, retrieval errors of SSS were around 0.64 and 0.63 psu for H and V polarizations, respectively. This result indicates that the effect of the foam layer on SSS retrieval with the low SST is greater than that of the high SST, owing to the weak sensitivity of sea surface brightness temperatures to SSS at the low SST. For a rough sea surface, emissivity of the flat surface can be replaced by that of a rough surface in Equation (11). This example indicates that the foam layer indeed generates a large error of SSS retrieval under high wind speeds and low SST, and should be considered in establishing a theoretical retrieval model of SSS. In addition, for the open ocean with high wind speeds, foam coverage fraction w is an important variable in retrieving SSS. From Equation (11), brightness temperature error $\Delta_w T_p$ induced by measured error Δw of foam coverage fraction can be calculated with the term of $\Delta w \Delta e_p^F T_{sea}$ (*i.e.*, $\Delta_w T_p = \Delta w \Delta e_p^F T_{sea}$). The SSS retrieval error will be estimated by $\Delta_w T_p$ divided by sensitivities of sea surface brightness temperatures to SSS.

6. Conclusions

At low SST, emissivity experiments of an artificial foam-covered sea surface at L-band were conducted for variable salinities and incidence angles. Emissivities were obtained from measured brightness temperatures of both foam-free and foamy surfaces. Based on the experimental data, the RM emissivity model was confirmed by well-known theoretical EMA models. In this experiment, the emissivity increments were from 0.016 to 0.161 for H polarization and 0.025 to 0.184 for V polarization. These emissivity increments indicate large retrieval error of SSS with sea surface brightness temperature at L-band under high wind speeds. Furthermore, the mechanism of emissivity increase of the foam-covered surface was investigated with both experimental data and a theoretical model. The results show that foam thickness, AVF, SSS and SST are important factors for predicting foam emissivities. The effects of AVF and foam thickness are stronger than those of SSS and SST. The theoretical RM emissivity model implies that at a fixed foam thickness, the emissivity increments increase with SSS increase and AVF decrease when the AVF is larger than 0.7. With the foam thickness increase, emissivity of the wave approach clearly fluctuates up to a specific saturation value, which depends on SST, SSS, AVF, and incidence angle. In addition, foam coverage fraction is also an important parameter of effecting SSS retrieval.

For the interface between the foam layer and water surface, we discussed contributions of the meniscus zone to the emissivity increments varying with microwave frequencies 1–37 GHz. The result indicates that the greatest contribution of the meniscus layer to emissivity increments of a 1.3 cm foam layer was at ~8 GHz. Stable ratios of emissivity increment of the meniscus to that of the foam layer

were about 36% for H polarization and 45% for V polarization, for frequencies between 20 and 37 GHz. However, at L-band (1.4 GHz), the meniscus had a weak effect on increasing the emissivity of the foam layer.

In summary, our experimental results are applicable to building an emissivity model of the sea surface with foam coverage and SSS retrieval model with satellite-observed brightness temperatures at L-band. To reduce brightness temperature error induced by the foam layer, the AVF and foam layer thickness are key parameters, owing to greater sensitivities of emissivity to them. However, for the complex microstructure of a foam layer, because the AVF and bubble size vary with foam layer depth, it is very difficult to measure the AVF exactly. Generally, AVF vertical distributions and the foam layer thickness depend on the dynamics of wave breaking on the ocean surface. To retrieve geophysical parameters from satellite data at various frequencies, spatiotemporal distributions of the AVF, foam thickness and foam coverage should be measured for the ocean.

Acknowledgments

The authors would like to thank the National Natural Sciences Foundation of China (grant number 41276183) and National 863 Project of China (grant number 2009AA09Z102) and Strategic Priority Research Program of the Chinese Academy of Sciences (grant number XDA11010104).

Author Contributions

En-Bo Wei conceived the study, carried out the experiment, collected and analyzed the data, and wrote the manuscript. Shu-Bo Liu validated the data analysis, executed the theoretical model and compiled the computer program. Zhen-Zhan Wang, Xiao-Lin Tong, Shuai Dong, Bin Li, and Jing-Yi Liu designed the L-band radiometer and performed experiments and data analyses. All authors complied with and approved the final manuscript.

Conflicts of Interest

The authors declare no conflict of interest.

References

1. Font, J.; Lagerloef, G.; le Vine, D.; Camps, A.; Zanife, O. The determination of surface salinity with the European SMOS space mission. *IEEE Trans. Geosci. Remote Sens.* **2004**, *42*, 2196–2205.
2. Lagerloef, G.; Colomb, F.R.; le Vine, D.; Went, Z.; Yueh, S.; Ruf, C.; Lilly, J.; Gunn, J.; Chao Y.; deCharon, A.; *et al*. The Aquarius/SAC-D Mission: Designed to meet the salinity remote sensing challenge. *Oceanography* **2008**, *21*, 68–81.
3. Anguelova, M.D. Complex dielectric constant of sea foam at microwave frequencies. *J. Geophys. Res.* **2008**, *113*, C08001.
4. Tang, C.C.H. The effect of droplets in the air-sea transition zone on the sea brightness temperature. *J. Phys. Oceanogr.* **1974**, *4*, 579–593.
5. Anguelova, M.D.; Gaiser, P.W. Microwave emissivity of sea foam layers with vertically inhomogeneous dielectric properties. *Remote Sens. Environ.* **2013**, *139*, 81–96.

6. Camps, A.; Vall-Liossera, M.; Reul, N.; Chapron, B.; Corbella, I.; Duffo, N.; Torres, F. The emissivity of foam-covered water surface at L-band: Theoretical modeling and experimental results from the frog 2003 field experiment. *IEEE Trans. Geosci. Remote Sens.* **2005**, *43*, 925–937.
7. Chen, D.; Tsang, L.; Zhou, L.; Reising, S.C.; Asher, W.E.; Rose, L.A.; Ding, K.H. Microwave emission and scattering of foam based on Monte Carlo simulations of dense media. *IEEE Trans. Geosci. Remote Sens.* **2003**, *41*, 782–789.
8. Rose, L.A.; Asher, W.E.; Reising, S.C.; Gaiser, P.W.; Germain, K.M.; Dowgiallo, D.J.; Horgan, K.A.; Farquharson, G.; Knapp, E.J. Radiometric measurements of the microwave emissivity of foam. *IEEE Trans. Geosci. Remote Sens.* **2002**, *40*, 2619–2625.
9. Wei, E.B. Microwave vector radiative transfer equation of a sea foam layer by the second-order Rayleigh approximation. *Radio Sci.* **2011**, *46*, RS5012–RS5013.
10. Wei, E.B. Effective Medium approximation model of sea foam layer microwave emissivity of a vertical profile. *Int. J. Remote Sens.* **2013**, *34*, 1180–1193.
11. Wei, E.B.; Liu, S.B.; Wang, Z.Z.; Liu, J.Y.; Dong, S. Emissivity measurements and theoretical model of foam-covered sea surface at C-band. *Int. J. Remote Sens.* **2014**, *35*, 1511–1525.
12. Smith, P.M. The emissivity of sea foam at 19 and 37 GHz. *IEEE Trans. Geosci. Remote Sens.* **1988**, *26*, 541–547.
13. Breward, C.J.W. The Mathematics of Foam. Ph.D. Thesis, University of Oxford, Oxford, UK, 1999.
14. Podzimek, J. Size spectra of bubbles in the foam patches and of sea salt nuclei over the surf zone. *Tellus* **1984**, *36*, 192–202.
15. Koehler, S.A.; Hilgenfeldt, S.; Stone, H.A. A generalized view of foam drainage: Experiment and theory. *Langmuir* **2000**, *16*, 6327–6341.
16. Stogryn, A. The emissivity of sea foam at microwave frequencies. *J. Geophys. Res.* **1972**, *77*, 1658–1666.
17. Guo, J.; Tsang, L; Asher, W.E.; Ding, K.H.; Chen, C.T. Applications of dense media radiative transfer theory for passive microwave remote sensing of foam covered ocean. *IEEE Trans. Geosci. Remote Sens.* **2001**, *39*, 1019–1027.
18. Wei, E.B.; Liu, Y. Application of effective medium approximation theory to ocean remote sensing under wave breaking. *Sci. China Ser. D Earth Sci.* **2007**, *50*, 474–480.
19. Wei, E.B.; Ge, Y. A microwave emissivity model of sea surface under wave breaking. *Chin. Phys.* **2005**, *14*, 1259–1264.
20. Liu, S.B.; Wei, E.B.; Jia, Y.X. Estimating microwave emissivity of sea foam by Rayleigh method. *J. Appl. Remote Sens.* **2013**, *7*, 073598.
21. Raizer, V.Y. Macroscopic foam-spray models for ocean microwave radiometry. *IEEE Trans. Geosci. Remote Sens.* **2007**, *45*, 3138–3144.
22. Ding, K.H.; Mandt, C.; Tsang, L.; Kong, J.A. Monte Carlo simulations of pair distribution function of dense discrete random media with multiple sizes of particles. *J. Electromagn. Waves Appl.* **1992**, *6*, 1015–1030.
23. Zhang, Y.; Yang, Y.E.; Kong, J.A. A composite model for estimation of polarimetric thermal emission from foam-covered wind-driven ocean surface. *Prog. Electromagn. Res.* **2002**, *37*, 143–190.

24. Padmanabhan, S.; Reising, S.C.; Asher, W.E.; Rose, L.A.; Gaiser, P.W. Effects of foam on ocean surface microwave emission inferred from radiometric observations of reproducible breaking wave. *IEEE Trans. Geosci. Remote Sens.* **2006**, *44*, 569–583.
25. Williams, G.F. Microwave emissivity measurements of bubbles and foam. *IEEE Trans. Geosci. Electron.* **1971**, *9*, 221–224.
26. Militskii, Y.A.; Raizer, V.Y.; Sharkov, E.A.; Etkin, V.S. Thermal radio emission from foam structures. *Sov. Phys.Tech. Phys. (Engl. Trans.)* **1978**, *23*, 601–602.
27. Boutin, J.; Martin, N.; Yin, X.B.; Font, J.; Reul, N.; Spurgeon, P. First assessment of SMOS data over open ocean: Part II Sea surface salinity. *IEEE Trans. Geosci. Remote Sens.* **2012**, *50*, 1662–1675.
28. Yueh, S.H.; West, R.; Wilson, W.J.; Li, F.K.; Njoku, E.G.; Rahmat-Smii, Y. Error source and feasibility for microwave remote sensing of ocean surface salinity. *IEEE Trans. Geosci. Remote Sens.* **2001**, *39*, 1049–1060.
29. Yueh, S.H.; Chaubell, J. Sea surface salinity and wind retrieval using combined passive and active L-band microwave observations. *IEEE Trans. Geosci. Remote Sens.* **2012**, *50*, 1022–1032.
30. Garnett, J.C.M. Colours in Metal Glasses, in Metallic Films, and in Metallic Solution. *Philos. Trans. R. Soc. A* **1906**, *205*, 237–288.
31. Blanch, S.; Aguasca, A. Dielectric permittivity measurements of sea water at L-band. In Proceedings of the First Results Workshop on EuroSTARRS, WISE, LOSAC Campaigns, Toulouse, France, 4–6 November 2002; Fletcher, P., Ed.; ESA Publications Division: Noordwijk, The Netherlands, 2003; ESA SP-525, pp. 137–141.
32. Tsang, L.; Kong, J.A.; Ding, K.H. Scattering and emission by layered media. In *Scattering of Electromagnetic Waves: Theories and Application*; John Wiley & Sons: New York, NY, USA, 2000; pp. 203–207.
33. Ulaby, F.T.; Moore, R.K.; Fung, A.K. Passive microwave sensing of the ocean. In *Microwave Remote Sensing: Active and Passive*; Artech House, Inc.: Dedham, MA, USA, 1986; Volume III, pp. 1440–1447.
34. Wilheit, T.T. A model for the microwave emissivity of the ocean's surface as a function of wind speed. *IEEE Trans. Geosci. Electron.* **1979**, *17*, 244–249.
35. Anguelova, M.D.; Gaiser, P.W. Skin depth at microwave frequencies of sea foam layers with vertical profile of void fraction. *J. Geophys. Res.* **2011**, *116*, C11002.
36. Monahan, E.C.; O'Muircheartaigh, I.G. Optimal power-law description of oceanic whitecap coverage dependence on wind speed. *J. Phys. Oceanogr.* **1980**, *10*, 2094–2099.